Revealing the Impact of Catalyst Phase Transition on Carbon Nanotube Growth by *in Situ* Raman Spectroscopy
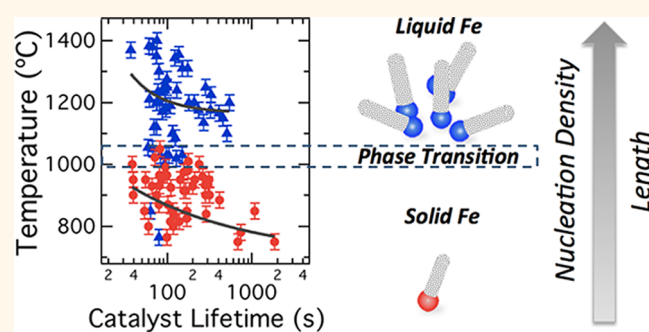
Rahul Rao,[†,‡,▽,*] Neal Pierce,[†,§] David Liptak,[†,⊥] Daylond Hooper,[†,⊥] Gordon Sargent,[†,⊥] S. Lee Semiatin,[†] Stefano Curtarolo,[¶] Avetik R. Harutyunyan,[#] and Benji Maruyama[†,*]

[†]Materials and Manufacturing Directorate, Air Force Research Laboratory, Wright-Patterson Air Force Base, Ohio 45433, United States , [‡]National Research Council, Washington, D.C. 20001, United States , [§]University of Dayton Research Institute, Dayton, Ohio 45469, United States , [⊥]UES Inc., Dayton, Ohio 45433, United States , [¶]Duke University, Durham, North Carolina 27708, United States , and [#]Honda Research Institute, Columbus, Ohio 43212, United States. [▽]Present address: Honda Research Institute, Columbus, Ohio 43212, United States.

ABSTRACT The physical state of the catalyst and its impact on the growth of single-walled carbon nanotubes (SWNTs) is the subject of a long-standing debate. We addressed it here using *in situ* Raman spectroscopy to measure Fe and Ni catalyst lifetimes during the growth of individual SWNTs across a wide range of temperatures (500−1400 °C). The temperature dependence of the Fe catalyst lifetimes underwent a sharp increase around 1100 °C due to a solid-to-liquid phase transition. By comparing experimental results with the metal−carbon phase diagrams, we prove that SWNTs can grow from solid *and* liquid phase-catalysts, depending on the temperature.

Carbon nanotubes are impressive because of their wide range of potential applications, from structural composites to energy storage to sensors and electronic devices.[1] However, their transition to commercial use is impeded by our continued inability to control growth. The lack of control largely stems from holes in our fundamental understanding of growth mechanisms. In this regard, one important issue that remains largely unresolved is the role of the physical state of the catalyst in influencing the structure and yield of SWNTs. While the state of the catalyst (*i.e.*, liquid or solid) during nanotube growth was long debated in the literature, growth from oxides,[2] carbides,[3,4] and low-melting temperature metals,[5] have shown that growth is possible from both liquids and solids. The state of the catalyst has important implications for both the resultant growth in terms of yield or length,[6,7] as well as our understanding of the growth mechanisms. For example, in the solid state, the catalyst can form facets, which may template[8,9] the carbon nanotube to grow preferentially metallic[10] or semiconducting nanotubes.[11] Diffusion mechanisms and solubility limits in liquid versus solid states are very different, and are important considerations in growth models; for example whether carbon diffuses in the bulk of the catalyst or along the surface.[12] However, the most interesting catalysts, that is, transition metals like Fe or Ni have solid-to-liquid transitions within the typical temperature range of SWNT growth. Thus we wondered how the state of the catalyst impacts the growth of carbon nanotubes and what the implications for this are on growth mechanisms.

To directly address this issue, here we used a unique system, the Adaptive Rapid Experimentation and Spectroscopy (ARES) system, which incorporated micro-Raman spectroscopy with cold-wall chemical vapor deposition (CVD), to measure the growth kinetics of individual SWNTs[13] from two of the most popular transition metal catalysts—Fe and Ni. *In situ* Raman spectroscopy during SWNT growth has
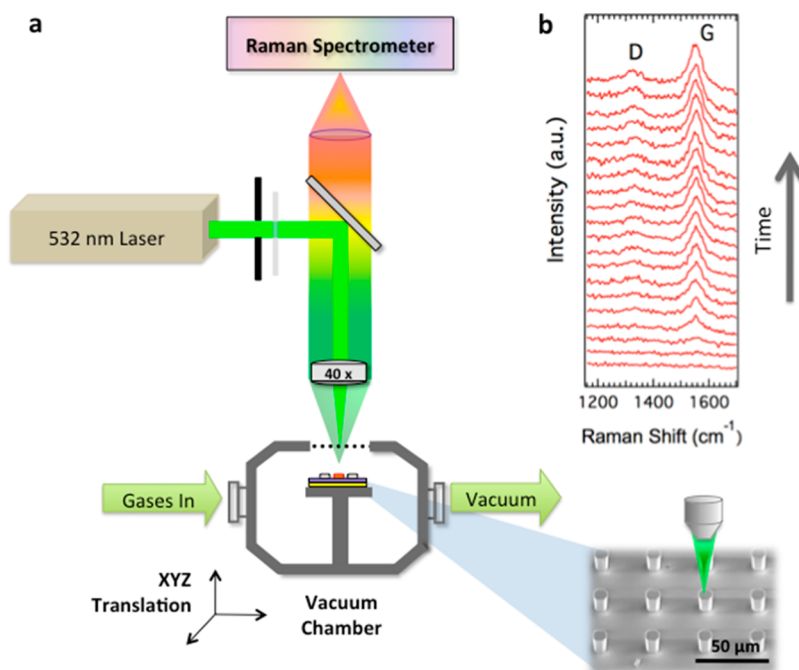
Figure 1. (a) Schematic of the adaptive rapid experimentation and spectroscopy (ARES) system used for *in situ* studies of SWNT catalyst lifetime. A magnified view of the pillars is shown in the SEM image on the bottom right. (b) Waterfall plot showing temporal evolution of Raman spectra from a growing nanotube in the D and G band region. Spectra averaged every 20 s from consecutive time windows are plotted from bottom to top.

previously been used successfully to evaluate growth kinetics of individual[13] and ensembles of SWNTs.[14−17] Here we were able to perform more than 100 experiments over a wide range of growth temperatures (500−1400 °C), enabling us to reveal striking differences between Fe and Ni with an unprecedented level of detail. The Fe catalyst lifetime exhibited a discontinuity with increasing growth temperatures and was accompanied by an increase in SWNT yield, indicating the first direct observation of growth across a solid− liquid phase transformation. Our results suggest that the length and nucleation efficiency of SWNTs can be controlled by engineering the phase states of the catalysts.

RESULTS AND DISCUSSION

Figure 1a shows a schematic of the ARES system used for the SWNT growth studies. The setup involved laser-induced heating (laser excitation = 2.33 eV) of catalyst films (Fe and Ni) on silicon pillars, which were formed by etching Si-on-SiO$_2$ wafers (see the magnified scanning electron microscopy (SEM) image on the bottom right in Figure 1a and the Methods section below for more details).[13] The small thermal mass of the pillars (10 μm diameter and height), combined with thermal isolation from the wafer due to the oxide barrier, enabled rapid heating to nanotube growth temperatures ranging from 500 to 1400 °C using ethylene as the hydrocarbon source. The light scattered from the pillars was collected for Raman spectra, which were acquired continuously during the growth

of SWNTs from within the laser spot. An example of a time-series of Raman spectra collected during a growth experiment with Fe catalyst is shown as a waterfall plot in Figure 1b, where initiation of SWNT growth is indicated by the appearance and subsequent increase in intensity of the G band at ~1560 cm^{-1} (downshifted due to the elevated temperature). The G band areas from each spectrum were calculated and plotted with respect to time in order to evaluate the growth kinetics of the SWNTs. The Raman spectra were also normalized with respect to the substrate (Si) peak intensities in order to enable fair comparison of the data across all the growth experiments. The Raman spectrum collected just before the appearance of the G band was assigned to the time corresponding to $t = 0$. We note that a few previous *in situ* growth studies have reported an "incubation time" during which the G band intensity increases slowly, followed by growth and termination phases.[15,18] Such an incubation time was not observed in this study.

The integrated G band areas (normalized to unity) from two different experiments (using Fe and Ni catalysts) are plotted with respect to time in Figure 2. The growth curves in Figure 2 were fitted to a decaying exponential growth equation of the form: $G(t) = \nu\tau[1 - \exp(-t/\tau)]$, where $G(t)$, ν, and τ are the area of the G band, initial growth rate, and time constant for the reaction, respectively.[13−17] The growth curves shown in Figure 2 panels a and b correspond to experiments conducted at different growth temperatures. It is clear from both Figure 2 that the growth curve
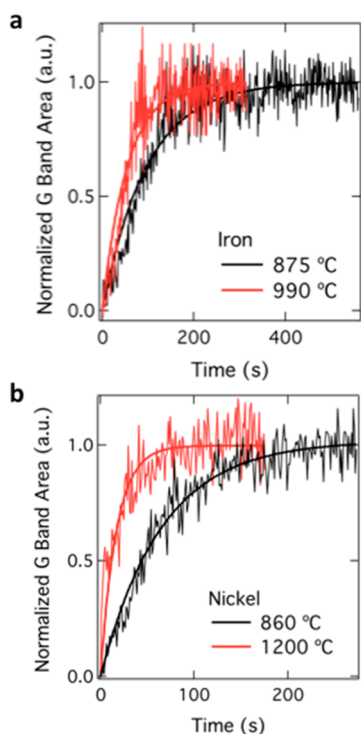
a

b

Figure 2. Typical growth curves at two different growth temperatures obtained by plotting the calculated G band area (normalized to unity) versus time, using (a) Fe, and (b) Ni catalysts. The growth curves are fitted to an exponential equation of the form $G(t) = \nu\tau[1 - \exp(-t/\tau)]$ where $G(t)$, ν, and τ are the area of the G band, initial growth rate and time constant of the reaction, respectively.

corresponding to the higher temperatures (990 °C for Fe and 1200 °C for Ni) has a smaller time constant—that is, growths at the higher temperatures terminated faster than growth at lower temperatures, implying that the catalyst had a shorter lifetime at the higher temperature. Henceforth, the time constants obtained from the fits to the growth curves will be referred to as the catalyst lifetimes.

In general, the lifetime of a thermally activated catalytic process is a function of the temperature. Lifetime values obtained from many different experiments using Fe and Ni catalysts are plotted against growth temperatures in Figure 3 panels a and c, respectively. Every data point in Figure 3a,c corresponds to a separate growth experiment; in all, over 100 experiments were performed over a wide temperature range from 500 to 1400 °C. Note the significant difference between the behaviors of Fe and Ni: While the Ni catalyst lifetimes decrease monotonically with temperature (Figure 3c), there is a discontinuity in the Fe case between 1000 and 1100 °C (Figure 3a) where the catalyst lifetime increases from ∼100 s to ∼600 s. From a thermodynamic perspective, the discontinuity in the lifetime of the Fe catalyst near 1100 °C (Figure 3a), that is, an abrupt increase with increasing temperature, is suggestive of a phase transition between

1000 and 1100 °C, thus implying a difference in the catalytic process at low and high temperatures.

The shaded band between 1000 and 1100 °C in Figure 3a delineates the transition between low and high temperature growth, referred to as regions I and II, respectively. The catalyst lifetimes decrease monotonically with increasing growth temperature in region I, followed by a transition between 1000 and 1080 °C, above which the catalyst lifetime jumps from ∼100 s up to ∼600 s. Beyond 1100 °C, the lifetime values decrease again up to the maximum growth temperature (∼1390 °C) in region II. The decrease in Fe catalyst lifetimes are also indicated by the exponential fits to the data in regions II and I in Figure 3a (also see Supporting Information, Figure S1 and related discussion regarding the data fits). In contrast to Fe, the Ni catalyst lifetimes decrease monotonically across the full temperature range (Figure 3c), and do not exhibit any discontinuity, suggesting the same phase of Ni catalyst at all growth temperatures. Unlike the catalyst lifetimes, the initial growth rates did not display any discontinuity for either Fe or Ni with increasing temperature (Supporting Information, Figure S2).

To understand the nature of this discontinuity in the Fe catalyst lifetime, we compare the Fe and Ni lifetime−temperature plots in Figure 3 panels a and c to their corresponding modified metal−carbon binary phase diagrams. It should be noted that our experimental results are based on reaction kinetics, while the phase diagrams correspond to thermodynamic equilibrium. Nevertheless, it is instructive to compare the evolution of the lifetimes with the thermodynamic phase diagrams for a qualitative understanding of the catalyst behavior. In Figure 3 panels b and d we show the Fe- and Ni-rich parts of the modified Fe−C and Ni−C phase diagrams, respectively. Both phase diagrams have been downshifted by $\Delta T \approx 125$ °C to account for the Gibbs−Thomson depression for a supported catalyst particle.[19,20] The initial particle size distributions of the as-deposited Fe and Ni deposition on the pillars were quite similar (see Supporting Information Figure S3), with a mean particle size around 2.5 nm, hence the shaded transition regions in Figure 3 to account for size-related effects.

When comparing the lifetime−temperature plot in Figure 3a with the modified Fe−C phase diagram (Figure 3b), it becomes immediately apparent that region I can be attributed to the phase fields below the eutectic temperature. This implies that the Fe-catalyst was in the solid state for growth temperatures up to 1000 °C. Interestingly, this range of temperatures is also the most common for SWNT growth. The Fe catalyst lifetimes experience a sharp increase from ∼100 s to ∼600 s as the growth temperature goes up to around 1100 °C. As mentioned above, discontinuities in thermal processes can be attributed to phase transitions. Indeed when compared with the modified
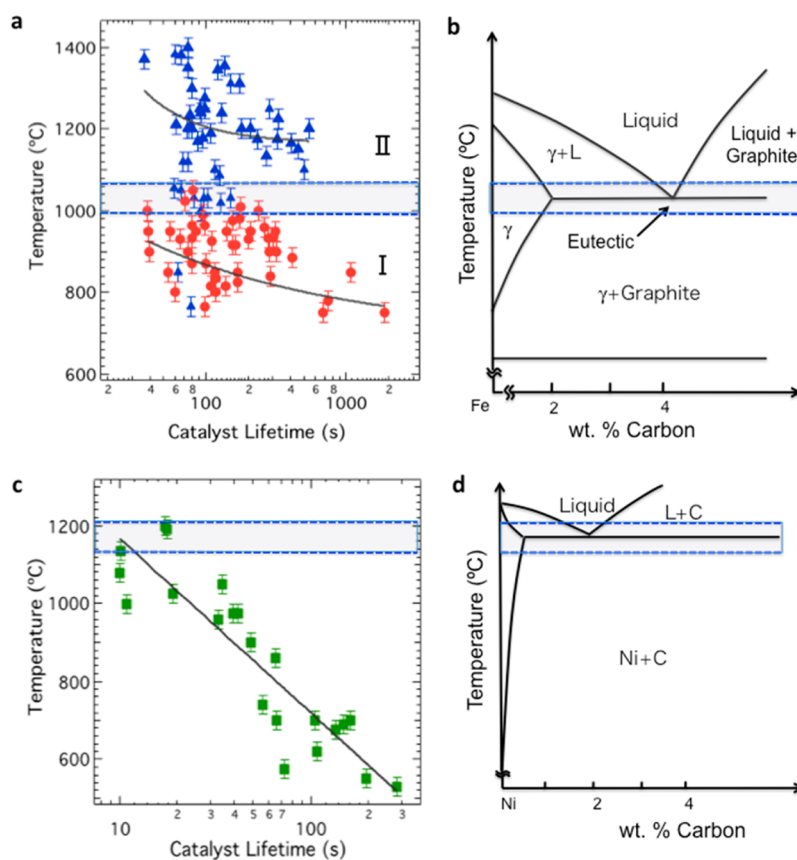
Figure 3. (a) Semilog plot of catalyst lifetimes vs growth temperatures for single SWNTs (circles) and multiple SWNTs (triangles) grown from Fe, and (b) the Fe-rich part of the modified Fe−C phase diagram. (c) Semilog plot of catalyst lifetimes vs growth temperatures for Ni, and (d) the Ni-rich part of the modified Ni−C phase diagram. The solid lines are exponential fits to the data. The shaded horizontal regions in the figures correspond to phase transitions in the modified binary phase systems. The horizontal and vertical error bars in panels a and c indicate a ±5% variability in catalyst lifetime values, and a ±25 °C uncertainty in temperature measurement, respectively.

phase diagram, one can see that region II is above the eutectic, implying that the Fe catalyst is in the liquid state in this region. We note that there is a large degree of scatter in the Fe lifetime data, which occurs due to a distribution in catalyst particle sizes (Supporting Information, Figure S3). Smaller diameter catalyst particles are highly reactive and can be deactivated more easily than larger particles,[21] leading to shorter lifetimes. Nonetheless, in spite of the scatter, the increase in Fe catalyst lifetimes between regions I and II is significant and likely due to a phase transformation.

Within region I or region II, the decrease in catalyst lifetimes with temperature could occur due to one or more termination mechanisms, namely, overcoating of the catalyst particle by carbon,[22,23] particle coarsening,[21] or subsurface diffusion.[24] The maximum growth temperature in region I was around 1000 °C, above the thermal decomposition temperature of our hydro-carbon feedstock (ethylene).[25] Thus the likelihood of excess carbon buildup at higher temperatures increases and could cause early termination of growth (short lifetime). Furthermore, particle coarsening *via* Ostwald ripening and sintering is known to terminate SWNT growth.[21] Coarsening is also a thermal process

and can be expected to be enhanced at higher growth temperatures, causing increased mass loss (or gain) in the active catalyst particle, and hence terminating growth at an earlier time compared to growth at lower temperatures.[26] Finally, we note that our substrate was silicon with a native oxide layer. Fe atoms are known to diffuse into the Si surface during SWNT growth.[24] Additionally, Fe and Ni particles are known to form silicides at the elevated growth temperatures,[27,28] which could cause early growth termination. While it is unclear which of these mechanisms was directly responsible for growth termination, a detailed study was beyond the scope of this paper.

The Ni−C phase diagram (Figure 3d) is less compli-cated than the Fe−C phase diagram. The eutectic point for bulk Ni−C is ∼170 °C higher than that of Fe−C (it occurs at 1326 °C,[29] and for our nanoparticles it is expected to be ∼1180 °C according to the G-T depression). We conclude that the Ni catalyst used for SWNT growth therefore remained in the solid state over the entire growth temperature range, which explains the monotonic decrease of catalyst lifetimes with increasing temperatures (similar to the decrease in lifetimes in region I of solid Fe, as seen in Figure 3b)
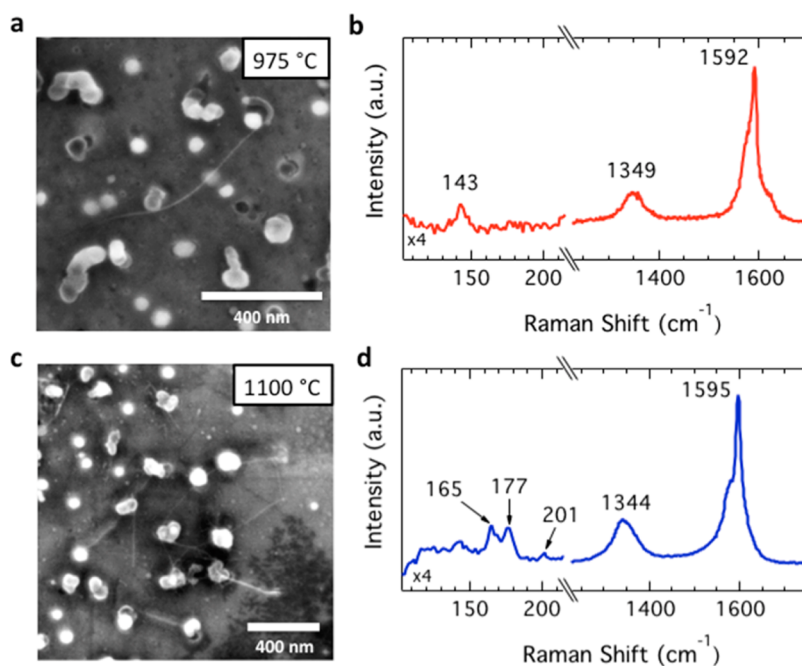
Figure 4. (a) SEM image and (b) postgrowth Raman spectrum of an individual SWNT grown under the laser spot from a Fe catalyst particle. A single peak in the low-frequency RBM region and a narrow G band identify the individual SWNT. (c) SEM image and (d) postgrowth Raman spectrum from a pillar where multiple SWNTs grew from Fe catalyst particles within the laser spot. The presence of multiple SWNTs is confirmed by the appearance of several RBMs, as well as a broader G band in the Raman spectrum.

and the absence of any discontinuities (phase transitions) in Ni. While we did not perform growths with Ni at temperatures beyond 1200 °C, it is worth noting that the behavior of the Ni serves as a useful reference for comparison with Fe and confirms the impact of the peculiarities of their phase diagrams on SWNT growth. The decrease of lifetimes with temperature can be attributed to reasons similar to the ones described above for Fe.

We performed SEM and *ex situ* Raman spectroscopy postgrowth to investigate differences between nanotubes grown from solid and liquid Fe, and solid Ni. SEM images collected from the Fe catalyst pillars with growth temperatures below 1000 °C (region I, Figure 3a) revealed that a majority contained only a single SWNT within the area heated by the laser,[13] while SEM images from the pillars corresponding to higher growth temperatures (region II) revealed the presence of multiple SWNTs grown within the area. Figure 4 panels a and c show examples of SEM images of growth experiments from regions I and II. The presence of an individual SWNT and multiple SWNTs can be clearly discerned at lower (Figure 4a) and higher (Figure 4c) growth temperatures, respectively. Further confirmation of this phenomenon was obtained by postgrowth Raman spectroscopy measurements. Figure 4 panels b and d show postgrowth Raman spectra collected from the areas corresponding to the SEM images in Figure 4 panels a and c, respectively. The Raman spectra (laser excitation 2.33 eV) exhibit peaks typical of SWNTs, namely, peaks in the low frequency

radial breathing mode (RBM) region, a disorder induced peak at ∼1345 cm^{-1}, and the graphitic G band at ∼1592 cm^{-1}.[30] The appearance of a single peak at 143 cm^{-1} in the RBM region in Figure 4b confirms the presence of a single SWNT on the pillar within the laser-irradiated zone. Additional support is provided by the narrow linewidths of the RBM (∼4 cm^{-1}) and the G band (∼8 cm^{-1}), which are characteristics of an individual SWNT.[31,32] In contrast, the Raman spectrum from the pillar that has multiple SWNTs (Figure 4c) exhibits RBMs at 165, 177, and 201 cm^{-1}, as well as a broader G band (∼14 cm^{-1}), confirming the presence of multiple SWNTs. We note that growth of a single SWNT under our synthesis conditions implies low nucleation efficiencies, the reasons for which are unclear at present. One possible reason could be the larger initial catalyst film thicknesses employed, which could significantly reduce the number of catalyst particles that are small enough to nucleate SWNTs. Nevertheless, it is important to stress that the low nucleation efficiencies enabled us to measure the growth kinetics of individual SWNTs, thereby giving us unique insights compared to the large numbers of nanotubes grown in forests.

We represent the occurrences of growth of single SWNTs with circles and multiple growths of SWNTs with triangles in Figure 3a. Interestingly, postgrowth SEM and Raman spectroscopy analysis on the Ni catalyst pillars showed only individual SWNTs on all the pillars (Supporting Information, Figure S4). The observation of single and multiple SWNTs in regions I
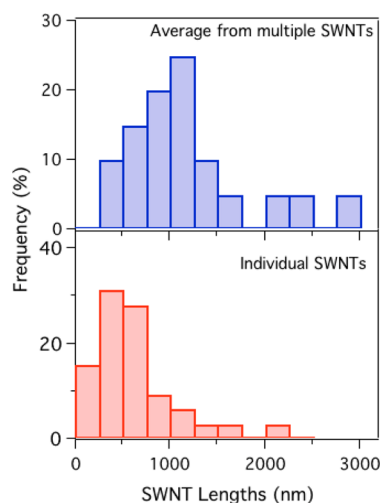
Figure 5. Histograms of lengths corresponding to individual SWNTs (bottom panel) grown at temperatures < 1100 °C (region I, Figure 3b) and multiple SWNTs (top panel) grown at temperatures > 1100 °C (region II, Figure 3b).

and II correlates very well with the phase transitions of the catalyst in regions I and II, implying that the solid catalyst produced single SWNTs for both Fe and Ni, while the nucleation density was higher with the liquid Fe catalyst, producing multiple SWNTs. Indeed, liquid Fe has a higher solubility for carbon, and hence probably a higher activity for SWNT growth. Furthermore, the diffusion of carbon through liquid Fe is faster than diffusion through solid γ-Fe (by 2 orders of magnitude),[33,34] thus the SWNTs grown from liquid Fe are expected to be longer.[6] SEM analysis revealed that the SWNTs in region II were generally longer than the SWNTs from region I (see histograms in Figure 5). We note that a detailed analysis of diffusion and reduction rates in solid and liquid Fe catalyst particles and their consequences toward nanotube growth would provide vital clues to prove the occurrence of a phase transition; such studies are currently in progress and will be reported in the future. We also note that the *in situ* growth curves measured from experiments that produced single and multiple SWNTs were fitted to a single exponential curve. In other words, in the experiments that produced multiple SWNTs, the lifetime

and initial growth rates are from the ensemble (see Supporting Information, Figure S5 and related discussion).

Finally, we point out another important difference between Fe and Ni—SWNT growth from Fe has longer lifetimes compared to that of Ni. Lifetimes up to 2000 s were observed in SWNTs growing from Fe, which is a factor of 6 higher than the longest lifetime observed for Ni. The diffusion of carbon in solid γ-Fe and solid Ni are of the same order of magnitude;[34,35] however, the solubilities of carbon in Fe and Ni are different. Although the carbon solubility has been predicted to reduce (Fe—C)[36] or increase (Ni—C)[37] *via* differing mechanisms due to the size reduction of nanoparticles, the values for the bulk systems can be used as a reasonable starting point. According to the bulk Fe—C and Ni—C phase diagrams,[29] the solvus of γ-Fe is ~4 times higher than that of Ni, making Fe more efficient at growing SWNTs, and could explain the longer lifetimes observed in Fe.

CONCLUSIONS

We used *in situ* Raman spectroscopy to measure the lifetimes of Fe and Ni catalysts over a wide range of growth temperatures. With our custom rapid experimentation (ARES) system, we carried out over 100 experiments, enabling us to glean important insights into the growth process that would have otherwise been missed. Our results revealed a discontinuity in the Fe catalyst lifetimes around 1100 °C due to a solid-to-liquid phase transition. In contrast, the monotonic behavior of the Ni lifetimes meant that Ni was in the solid state through the whole range of growth temperatures. The behavior of the Fe catalyst was explained by comparison with the binary metal—carbon phase diagrams, as well as experimental evidence, which showed dramatic increases in the nucleation densities and longer lifetimes when crossing the phase boundary from solid to the liquid state. Our results prove that SWNT growth is feasible from both solid and liquid catalyst depending on the growth temperature, resolving a long-standing debate in the field. As a direct consequence, the length and nucleation density of the SWNTs can be tailored for specific applications by engineering the correct catalyst and growth temperature.

METHODS

Growth of the SWNTs took place *via* laser-induced CVD inside a high vacuum chamber coupled to a Raman microscope, as shown schematically in Figure 1. The samples consisted of silicon pillars, 10 μm in diameter, spaced 40 μm apart, formed by deep reactive ion etching of a 10 μm top layer of a silicon-on-insulator substrate. The small thermal mass of the pillar allowed for efficient heating to the growth temperature (from 500 to 1400 °C) using a few hundred milliwatts of laser power. The oxide barrier layer below the pillars enhanced heating by restricting conductive heat transfer between the pillar and the underlying bulk silicon substrate. Thin films (2−3 nm) of Fe and Ni, sputtered on the substrates were used as catalysts for

nanotube growth. Prior to each growth experiment, the chamber was pumped down to a base pressure of ~9 × 10^{-6} Torr, followed by backfilling argon to the growth pressure of 25 Torr. At this time a constant flow of argon and hydrogen was initiated at 25 and 10 sccm, respectively, while the chamber pressure was maintained at 25 Torr. The Raman excitation laser was focused on each pillar through a long working distance 40× objective lens and heating was achieved by increasing the laser power. The temperature of the silicon pillars was estimated using the ratio of the anti-Stokes to Stokes peaks in the Raman spectra from the pillars.[38] Once the laser was focused on a pillar, the power was increased to heat it up to the growth temperature, followed by the introduction of 5 sccm of ethylene to initiate nanotube growth. Raman spectra between −2000 and 3000 cm^{-1}

were collected and saved at one-second intervals during the growth experiment. Nanotube nucleation and growth was detected by the appearance, and subsequent increase in intensity, of the G band at $1500-1600$ cm^{-1}. The ethylene flow was turned off after the G band intensity stabilized following the initial increase, thus indicating termination of growth.

REFERENCES AND NOTES

1. Baughman, R. H.; Zakhidov, A. A.; de Heer, W. A. Carbon Nanotubes—The Route toward Applications. *Science* **2002**, *297*, 787.
2. Steiner, S. A.; Baumann, T. F.; Bayer, B. C.; Blume, R.; Worsley, M. A.; MoberlyChan, W. J.; Shaw, E. L.; Schlogl, R.; Hart, A. J.; Hofmann, S.; *et al.* Nanoscale Zirconia as a Nonmetallic Catalyst for Graphitization of Carbon and Growth of Single- and Multiwall Carbon Nanotubes. *J. Am. Chem. Soc.* **2009**, *131*, 12144–12154.
3. Yoshida, H.; Takeda, S.; Uchiyama, T.; Kohno, H.; Homma, Y. Atomic-Scale *in-Situ* Observation of Carbon Nanotube Growth from Solid State Iron Carbide Nanoparticles. *Nano Lett.* **2008**, *8*, 2082–2086.
4. Wirth, C. T.; Bayer, B. C.; Gamalski, A. D.; Esconjauregui, S.; Weatherup, R. S.; Ducati, C.; Baehtz, C.; Robertson, J.; Hofmann, S. The Phase of Iron Catalyst Nanoparticles During Carbon Nanotube Growth. *Chem. Mater.* **2012**, *24*, 4633–4640.
5. Rao, R.; Eyink, K. G.; Maruyama, B. Single-Walled Carbon Nanotube Growth from Liquid Gallium and Indium. *Carbon* **2010**, *48*, 3971–3973.
6. Harutyunyan, A.; Tokune, T.; Mora, E. Liquid as a Required Catalyst Phase for Carbon Single-Walled Nanotube Growth. *Appl. Phys. Lett.* **2005**, *87*, 051919.
7. Cervantes-Sodi, F.; McNicholas, T. P.; Simmons, J. G., Jr.; Liu, J.; Csányi, G.; Ferrari, A. C.; Curtarolo, S. Viscous State Effect on the Activity of Fe Nanocatalysts. *ACS Nano* **2010**, *4*, 6950–6956.
8. Reich, S.; Li, L.; Robertson, J. Control the Chirality of Carbon Nanotubes by Epitaxial Growth. *Chem. Phys. Lett.* **2006**, *421*, 469–472.
9. Koziol, K. K. K.; Ducati, C.; Windle, A. H. Carbon Nanotubes with Catalyst Controlled Chiral Angle. *Chem. Mater.* **2010**, *22*, 4904–4911.
10. Harutyunyan, A. R.; Chen, G.; Paronyan, T. M.; Pigos, E. M.; Kuznetsov, O. A.; Hewaparakrama, K.; Kim, S. M.; Zakharov, D.; Stach, E. A.; Sumanasekera, G. U. Preferential Growth of Single-Walled Carbon Nanotubes with Metallic Conductivity. *Science* **2009**, *326*, 116–120.
11. Chiang, W.-H.; Sankaran, R. M. Linking Catalyst Composition to Chirality Distributions of as-Grown Single-Walled Carbon Nanotubes by Tuning Nixfe1-X Nanoparticles. *Nat. Mater.* **2009**, *8*, 1–5.
12. Hofmann, S.; Csányi, G.; Ferrari, A. C.; Payne, M. C.; Robertson, J. Surface Diffusion: The Low Activation Energy Path for Nanotube Growth. *Phys. Rev. Lett.* **2005**, *95*, 036101.
13. Rao, R.; Liptak, D.; Cherukuri, T.; Yakobson, B. I.; Maruyama, B. *In Situ* Evidence for Chirality-Dependent Growth Rates of Individual Carbon Nanotubes. *Nat. Mater.* **2012**, *11*, 1–4.
14. Picher, M.; Anglaret, E.; Arenal, R.; Jourdain, V. Self-Deactivation of Single-Walled Carbon Nanotube Growth Studied by *in Situ* Raman Measurements. *Nano Lett.* **2009**, *9*, 542–547.
15. Li-Pook-Than, A.; Lefebvre, J.; Finnie, P. Phases of Carbon Nanotube Growth and Population Evolution from *in Situ* Raman Spectroscopy During Chemical Vapor Deposition. *J. Phys. Chem. C* **2010**, *114*, 11018–11025.
16. Chiashi, S.; Murakami, Y.; Miyauchi, Y.; Maruyama, S. Cold Wall CVD Generation of Single-Walled Carbon Nanotubes and *in Situ* Raman Scattering Measurements of the Growth Stage. *Chem. Phys. Lett.* **2004**, *386*, 89–94.
17. Einarsson, E.; Murakami, Y.; Kadowaki, M.; Maruyama, S. Growth Dynamics of Vertically Aligned Single-Walled Carbon Nanotubes from *in Situ* Measurements. *Carbon* **2008**, *46*, 923–930.
18. Wako, I.; Chokan, T.; Takagi, D.; Chiashi, S.; Homma, Y. Direct Observation of Single-Walled Carbon Nanotube Growth Processes on SiO$_2$ Substrate by *in Situ* Scanning Electron Microscopy. *Chem. Phys. Lett.* **2007**, *449*, 309–313.
19. Jiang, A.; Awasthi, N.; Kolmogorov, A. N.; Setyawan, W.; Börjesson, K.; Bolton, K.; Harutyunyan, A. R.; Curtarolo, S. Theoretical Study of the Thermal Behavior of Free and Alumina-Supported Fe-C Nanoparticles. *Phys. Rev. B* **2007**, *75*, 205426.
20. Harutyunyan, A. R.; Mora, E.; Tokune, T.; Bolton, K.; Rosén, A.; Jiang, A.; Awasthi, N.; Curtarolo, S. Hidden Features of the Catalyst Nanoparticles Favorable for Single-Walled Carbon Nanotube Growth. *Appl. Phys. Lett.* **2007**, *90*, 3120.
21. Amama, P. B.; Pint, C. L.; McJilton, L.; Kim, S. M.; Stach, E. A.; Murray, P. T.; Hauge, R. H.; Maruyama, B. Role of Water in Super Growth of Single-Walled Carbon Nanotube Carpets. *Nano Lett.* **2009**, *9*, 44–49.
22. Puretzky, A. A.; Geohegan, D. B.; Jesse, S.; Ivanov, I. N.; Eres, G. *In Situ* Measurements and Modeling of Carbon Nanotube Array Growth Kinetics During Chemical Vapor Deposition. *Appl. Phys. A: Mater. Sci. Process.* **2005**, *81*, 223–240.
23. Yamada, T.; Maigne, A.; Yudasaka, M.; Mizuno, K.; Futaba, D. N.; Yumura, M.; Iijima, S.; Hata, K. Revealing the Secret of Water-Assisted Carbon Nanotube Synthesis by Microscopic Observation of the Interaction of Water on the Catalysts. *Nano Lett.* **2008**, *8*, 4288–4292.
24. Kim, S. M.; Pint, C. L.; Amama, P. B.; Zakharov, D. N.; Hauge, R. H.; Maruyama, B.; Stach, E. A. Evolution in Catalyst Morphology Leads to Carbon Nanotube Growth Termination. *J. Phys. Chem. Lett.* **2010**, *1*, 918–922.
25. Kamat, P. V. Graphene-Based Nanoarchitectures. Anchoring Semiconductor and Metal Nanoparticles on a Two-Dimensional Carbon Support. *J. Phys. Chem. Lett.* **2009**, *1*, 520–527.
26. Picher, M.; Anglaret, E.; Arenal, R.; Jourdain, V. Processes Controlling the Diameter Distribution of Single-Walled Carbon Nanotubes During Catalytic Chemical Vapor Deposition. *ACS Nano* **2011**, *5*, 2118–2125.
27. Simmons, J. M.; Nichols, B. M.; Marcus, M. S.; Castellini, O. M.; Hamers, R. J.; Eriksson, M. A. Critical Oxide Thickness for Efficient Single-Walled Carbon Nanotube Growth on Silicon Using Thin SiO$_2$ Diffusion Barriers. *Small* **2006**, *2*, 902–909.
28. Jung, Y. J.; Wei; Vajtai, R.; Ajayan, P. M.; Homma, Y.; Prabhakaran, K.; Ogino, T. Mechanism of Selective Growth of Carbon Nanotubes on SiO$_2$/Si Patterns. *Nano Lett.* **2003**, *3*, 561–564.
29. *Binary Alloy Phase Diagams*, 2nd ed.; Massalski, T. B., Okamoto, H., Eds.; ASM International Materials: Park, OH, 1990.
30. Jorio, A.; Dresselhaus, M. S.; Saito, R. *Raman Spectroscopy in Graphene Related Systems: Carbon Nanotubes, Nanographite and Graphene*; Wiley-VCH: Weinheim, Germany, 2011.
31. Rao, R.; Menendez, J.; Poweleit, C. D.; Rao, A. M. Anharmonic Phonon Lifetimes in Carbon Nanotubes: Evidence for a One-Dimensional Phonon Decay Bottleneck. *Phys. Rev. Lett.* **2007**, *99*, 047403–047404.
32. Jorio, A.; Fantini, C.; Dantas, M.; Pimenta, M.; Souza Filho, A.; Samsonidze, G.; Brar, V.; Dresselhaus, G.; Dresselhaus, M.; Swan, A.; *et al.* Linewidth of the Raman Features of Individual Single-Wall Carbon Nanotubes. *Phys. Rev. B* **2002**, *66*, 115411.

33. Goldberg, D.; Belton, G. The Diffusion of Carbon in Iron-Carbon Alloys at 1560°C. *Met. Mater. Trans. B* **1974**, *5*, 1643–1648.

34. Tibbetts, G. G. Diffusivity of Carbon in Iron and Steels at High Temperatures. *J. Appl. Phys.* **1980**, *51*, 4813–4816.

35. Xiang, Q.; Yu, J.; Jaroniec, M. Synergetic Effect of MoS_2 and Graphene as Cocatalysts for Enhanced Photocatalytic H_2 Production Activity of TiO_2 Nanoparticles. *J. Am. Chem. Soc.* **2012**, *134*, 6575–6578.

36. Harutyunyan, A. R.; Awasthi, N.; Jiang, A.; Setyawan, W.; Mora, E.; Tokune, T.; Bolton, K.; Curtarolo, S. Reduced Carbon Solubility in Fe Nanoclusters and Implications for the Growth of Single-Walled Carbon Nanotubes. *Phys. Rev. Lett.* **2008**, *100*, 195502.

37. Diarra, M.; Zappelli, A.; Amara, H.; Ducastelle, F.; Bichara, C. Importance of Carbon Solubility and Wetting Properties of Nickel Nanoparticles for Single Wall Nanotube Growth. *Phys. Rev. Lett.* **2012**, *109*, 185501.

38. Hart, T.; Aggarwal, R.; Lax, B. Temperature Dependence of Raman Scattering in Silicon. *Phys. Rev. B* **1970**, *1*, 638–642.